inorganics

MDPI

Article

A Tetranuclear Dysprosium Schiff Base Complex Showing Slow Relaxation of Magnetization

Mamo Gebrezgiabher [1,2], Sören Schlittenhardt [3], Cyril Rajnák [2], Assefa Sergawie [1], Mario Ruben [3,4,5,*], Madhu Thomas [1,*] and Roman Boča [2]

[1] Department of Industrial Chemistry, College of Applied Sciences and Nanotechnology Excellence Center, Addis Ababa Science and Technology University, Addis Ababa P.O. Box 16417, Ethiopia; mamo.gebrezgiabher@aastu.edu.et (M.G.); assefa.sergawie@aastu.edu.et (A.S.)
[2] Department of Chemistry, Faculty of Natural Sciences, University of SS Cyril and Methodius, 91701 Trnava, Slovakia; cyril.rajnak@ucm.sk (C.R.); roman.boca@ucm.sk (R.B.)
[3] Institute of Nanotechnology, Karlsruhe Institute of Technology, Hermann-von-Helmholtz-Platz 1, 6344 Karlsruhe, Germany; soeren.schlittenhardt@kit.edu
[4] Institute of Quantum Materials and Technologies (IQMT), Karlsruhe Institute of Technology, Hermann-von-Helmholtz-Platz 1, 76344 Karlsruhe, Germany
[5] Centre Européen de Science Quantique (CESQ), Institut de Science et d'Ingénierie Supramoléculaires (ISIS, UMR 7006), CNRS-Université de Strasbourg, 8 Allée Gaspard Monge, BP 70028, CEDEX, 67083 Strasbourg, France
* Correspondence: mario.ruben@kit.edu (M.R.); madhu.thomas@aastu.edu.et (M.T.)

Abstract: A tetranuclear dysprosium Schiff base complex was isolated by reacting dysprosium chloride with 2-hydroxy-3-methoxybenzaldehyde and 2-(aminomethyl)pyridine in-situ under basic conditions. The isolated Dy(III) complex was characterized by elemental analyses, single crystal X-ray diffraction and molecular spectroscopy. The complex crystallizes in the triclinic space group P-1 with unit cell parameters of a = 10.2003 (4), b = 13.8602 (5), c = 14.9542 (6), α = 94.523 (3), β = 109.362 (4), and γ = 99.861 (3). The magnetic properties of **1** have been investigated by DC and AC susceptibility measurements. The DC measurements reveal weak exchange coupling of antiferromagnetic nature. In the AC measurement, the complex shows a slow relaxation of magnetization in the absence of an external magnetic field.

Keywords: Schiff base; dysprosium complex; X-ray structure; slow magnetic relaxation

Citation: Gebrezgiabher, M.; Schlittenhardt, S.; Rajnák, C.; Sergawie, A.; Ruben, M.; Thomas, M.; Boča, R. A Tetranuclear Dysprosium Schiff Base Complex Showing Slow Relaxation of Magnetization. *Inorganics* **2022**, *10*, 66. https://doi.org/10.3390/inorganics10050066

Academic Editor: Ashley Wooles

Received: 26 April 2022
Accepted: 19 May 2022
Published: 21 May 2022

1. Introduction

Single molecule magnets (SMMs) are individual molecular compounds that exhibit slow relaxation of magnetization at zero field [1] below a certain temperature, which is called the blocking temperature [2]. Such slow relaxation is achieved by magnetic anisotropy causing an effective energy barrier U_{eff} to spin reversal. Mechanisms to overcome the barrier include spin-lattice processes (Ram, Orb, Direct) or quantum tunneling of magnetization (QTM) [3].

After the first SMM, $[Mn_{12}O_{12}(O_2CMe)_{16}(H_2O)_4]$ [4], was discovered, high spin, strongly coupled 3d transition metal complexes were initially considered to have the most potential for the development of SMMs. However, it has been confirmed over recent years that the f-block elements can also be used, which is based on the interaction between the electron density of the 4f ions and the crystal field environments in which it is placed. Lanthanides-based SMMs entered the field in 2003 with the report on the slow relaxation of magnetization in the $LnPc_2$ double-decker complexes [5], and hundreds of lanthanide SMMs were reported then after [6–18].

Due to their molecular properties, such as solubility, crystallinity, and so forth, SMMs have been proposed as promising candidates for various modern technological advancements, such as information and data storage as well as molecular spin qudits for quantum

algorithms [19] The coordination chemistry of Ln(III) ions has attracted the interest of many researchers for their ability to form clusters (polynuclear) with unprecedented and nanosized structures [20]. Lanthanide-based SMMs received special attention in molecular magnetism on account of their large spin state and high magnetic anisotropy [21].

Schiff bases are ideal candidates because of their fine tunability for the ligand field by varying substituents of both aldehyde and amine precursors [22,23]. Schiff base ligands containing two coordination pockets are believed to be effective for the preparation of heterometallic transition–lanthanide(3d-4f) single molecule magnets by forming individual pockets for 3d and 4f metal ions. These kinds of single molecule magnets are obtained by the exchange coupling of both 3d and 4f ions through oxide, hydroxide, or alkoxide bridges in the ligands. In the present study, we aimed at occupying both coordination pockets with dysprosium to try to understand their exchange coupling, which indeed led to the generation of a single molecule magnet.

Previous studies showed that the Schiff base ligand (HL) in the present study has been used to generate mixed metal isostructural hexanuclear Zn_2Ln_4 [24], dinuclear dysprosium [25], tetranuclear dysprosium cluster [26], copper [27], and palladium [28] complexes.

Here, we are reporting a novel pure 4f lanthanide compound with the formula of $C_{56}H_{54}Cl_6Dy_4N_8O_{10}$ (**1**) which synthesized by the in situ condensation of *o*-vanillin with 2-(aminomethyl)pyridine in the presence of triethylamine. Single-crystal XRD and magnetic studies reveal that it is a tetranuclear dysprosium Schiff base complex with weak magnetic exchange. Frequency-dependent AC susceptibility measurements suggest SMM behavior having a slow relaxation of magnetization at lower and higher frequencies.

2. Results and Discussion

2.1. Structural Description of Tetranuclear Dysprosium Complex **1**

Single crystal XRD studies confirm that complex **1** crystallizes in triclinic space group P-1 with half the molecule in the asymmetric unit (Figure 1a). The aggregate forms a dicationic planar tetranuclear dysprosium complex $[(Dy_4(L)_4\ (\mu_2\text{-}OH)_2Cl_4]^{2+}$ (Figure 1 and Scheme 1). In total, the molecule consists of four Dy(III) ions (Dy1, Dy2 and their symmetry equivalents (Dy1* (1-x, 1-y, 1-z), Dy2*(1-x, 1-y, 1-z)), four tetradentate Schiff base ligands (L^-), two bridging hydroxo, two bridging and two terminating chlorido ligands. The four Dy(III) ions are held together by four deprotonated Schiff base ligands (L^-), two (μ_2-OH) and two (μ_2-chloro). The other coordination sphere is completed by one chlorido ligand for Dy2 and Dy2*, respectively. The charge on the Schiff base complex is balanced by two chloride anions located outside of the sphere. The Schiff base ligand (HL) (Scheme 2a) adopts different bridging behavior of μ-1, μ-2, μ-1, μ-1 respectively after deprotonating (L^-) for Dy1 and Dy2, as shown in Scheme 2b,c, respectively. In a nutshell, the Schiff base ligand is acting in both chelating and bridging mode in the molecular structure of complex **1** (Figure 1b).

The four Dy(III) ions of the core almost lie on one plane, and the compound exhibits a planar butterfly-type structural topology. The metal center Dy1 and its symmetry equivalent Dy1* define the body of the butterfly, and Dy2 and its symmetry equivalent Dy2* define the wing tips of the butterfly motif (Figure 1b–d). The body and wing tips of the butterfly core are connected through the two μ_3-OH bridges. These bridging ligands are located above and below the plane. The peripheral part of the metal hydroxo cores are being bridged by four Schiff base ligands and two chloro ligands. Dy2 is connected to Dy1 via one phenoxido oxygen (O4) of one independent Schiff base ligand. Dy2 and Dy2* are further coordinated by one chlorido ligand (Cl2, Cl2*), respectively.

The bond distances of Dy2-O1 and Dy1–O1 are 2.379 (4) Å and 2. 295 (4) Å, respectively. Taking one of the half asymmetric molecular units, the bond angles of Dy1*–Cl1–Dy2, Dy1*–O2–Dy2, Dy1*–O1–Dy2, Dy2–O1–Dy1, Dy2–O4–Dy1 and Dy1*–O1–Dy1 are 80.12 (3)°, 99.6 (1)°, 100.0 (1)°, 107.3 (1)°, 112.6 (1)° and 108.9 (1)°, respectively (Table S1). The central dysprosium atoms Dy1 and Dy1* and the outer Dy2 and Dy2* are eight coordinate: with four oxygen, two chlorine and two nitrogen atoms for Dy2 and Dy2* and with five oxygen,

one chlorine and two nitrogen atoms for Dy1 and Dy1*. Calculations utilizing the shape v2.1 program [29] show that the coordination polyhedra of the two Dy(III)-ion central atoms in complex **1** belong to biaugmented trigonal prism (BTP) geometry (8-BTP, C_{2v}, 2.303) (Figure 2d, Table S3). Therefore, each eight-coordinate Dy(III) ion possesses a distorted biaugmented trigonal prism (BTP) geometry (Figure 2d) with a N_2O_5Cl coordination environment for Dy1 and Dy1* and $N_2O_4Cl_2$ coordination environment for Dy2 and Dy2*. The two square bases of the biaugmented trigonal prism for Dy2 comprise 01, O2, O3, O4, N3 and N4, respectively. However, for Dy1, the two square bases are well-defined by the atoms of O1, O1*, O2, O4, O5, N1 and N2 respectively (Figure 2). The complex under investigation is somewhat close to previously reported planar tetranuclear lanthanide hydroxo aggregates in terms of their bond distances and bond angles [30–36]. Wang et al. [26] have reported a planar tetranuclear dysprosium mixed ligand Schiff base aggregate, generating somewhat the same topology close to our report. The main difference between the two structures are on the coordination environment around the dysprosium metal ions. However, in both the aggregates, each Dy(III) ion possesses an eight-coordinated biaugmented trigonal prism (BTP) geometry as a common and additionally a triangular dodecahedron geometry in the reported structure of Wang et al. In addition to the preparative similarity, the similarities in the Dy–O, Dy–N, and Dy–Dy bond distances are also noticeable.

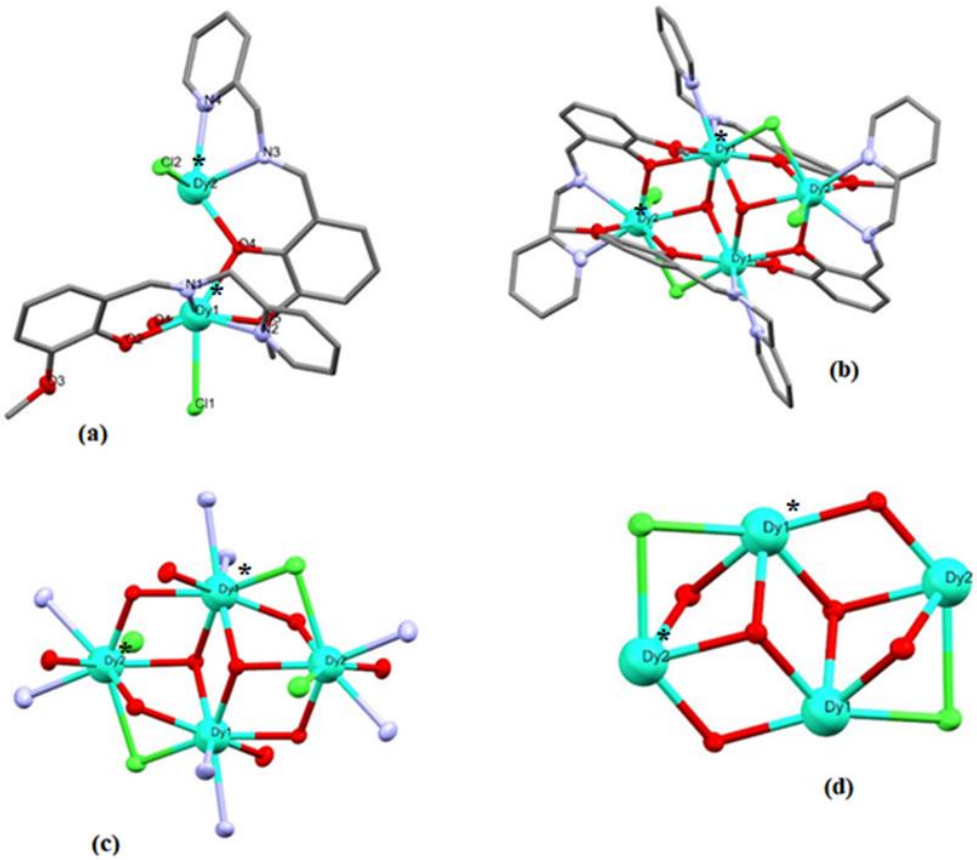

Figure 1. (**a**) Asymmetric unit of complex **1** (**b**) Full molecular structure of complex **1**; (**c**) The dysprosium core structure with coordinating atoms from each ligand for complex **1** (**d**) The dysprosium central core of complex **1**: Carbon atoms in (**c**,**d**) and hydrogen atoms in all the figures are omitted for clarity. Symmetry code (1-x, 1-y, -z). Color codes: cyan **Dy**(III), red **O**, black **C**, blue **N**, and green **Cl** and * represents symmetry generated atom.

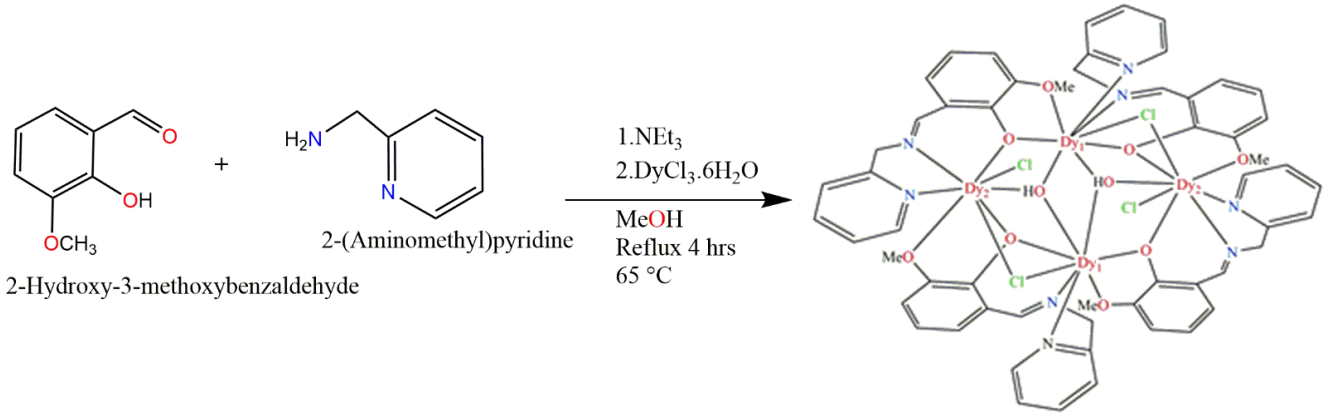

Scheme 1. Schematic representation of the reaction procedure for complex **1**.

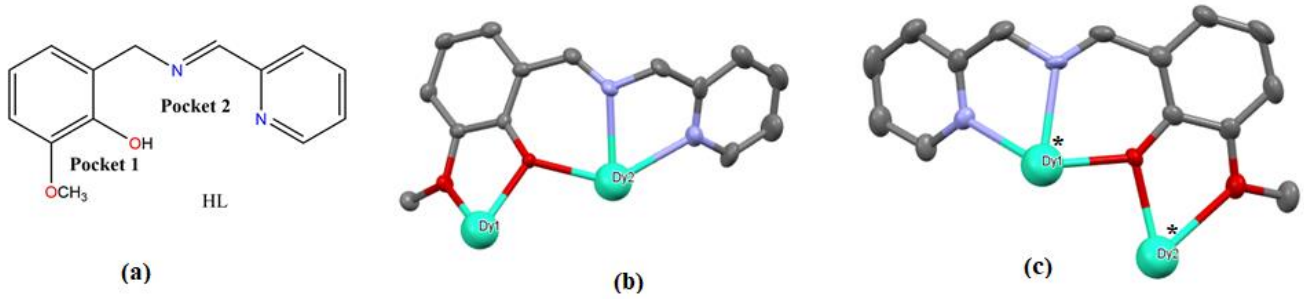

Scheme 2. This Structure of the Schiff base ligand HL (**a**) and its binding modes after deprotonation (L^-) (**b**,**c**) with Dy1 and Dy2, Dy1*, and Dy2* is in coordination mode of μ-1, μ-2, μ-1, μ-1. All hydrogen atoms in (**b**,**c**) are removed for clarity. Color codes: cyan **Dy**(III), red **O**, black and * represents symmetry generated atom.

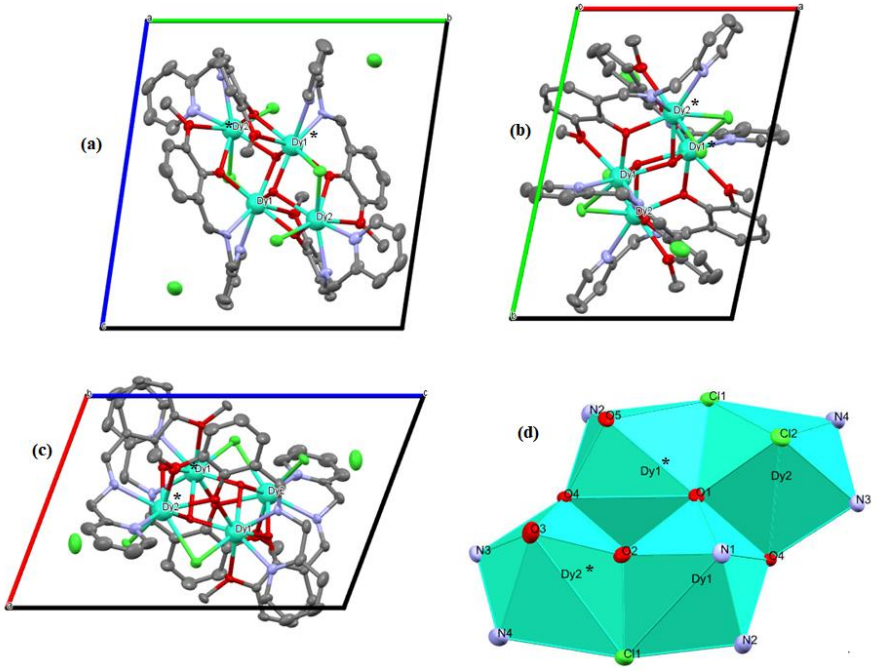

Figure 2. Molecular packing arrangements along the crystallographic (**a**) a-axis (**b**) b-axis and (**c**) c-axis (**d**) Coordination polyhedra of distorted biaugmented trigonal prism (BTP) geometry observed for Dy(III) ion in complex **1**. All hydrogen atoms are omitted for clarity. Color codes: cyan **Dy**(III), red **O**, black, **C** and green **Cl**.

From the unit cell packing, it has been revealed that there is one molecule exiting per unit cell (Figure 2a–c) without hydrogen bonding. However, there are several intermolecular connections happening in the molecule in the unit cell of half of the asymmetric unit. The bond distances observed in the intermolecular contacts/bonding in H26–Cl3, H23A–Cl3, H15–Cl1, H15A–Cl2, C15–Cl1 and H8–Cl3 are in the range of 2.760–3.255 Å. The molecular packing of the extended network in different directions is shown in Figure S1.

2.2. DC Susceptibility

The temperature dependence of the magnetic susceptibility for **1** was taken between T = 2 and 300 K at the magnetic field B_{DC} = 0.1 T. Raw data were corrected for the estimated underlying diamagnetism and transformed to the dimensionless product function $\chi T/C_0$ ($C_0 = N_A\mu_0\mu_B^2/k_B$ is the reduced Curie constant containing only the fundamental physical constants in their usual meaning) that is displayed in Figure 3.

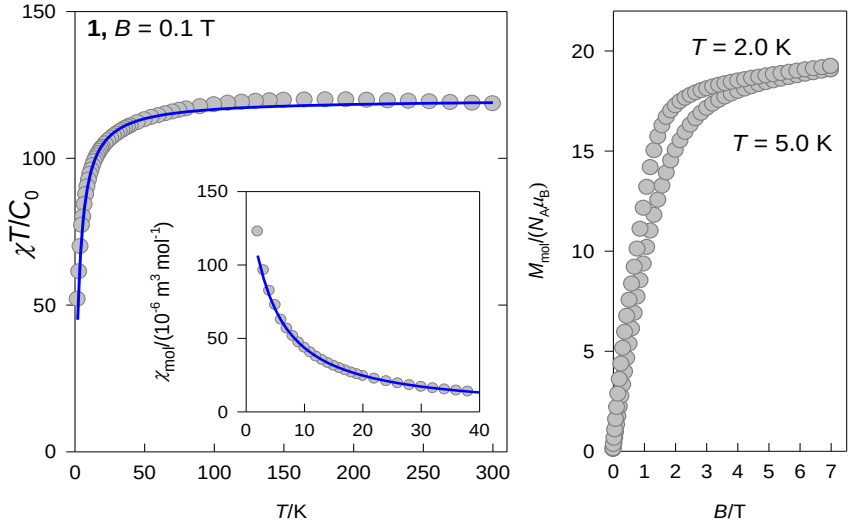

Figure 3. Plot of the χT vs. T for **1** in an applied magnetic field of B_{DC} = 0.1 T. Solid lines—fitted (see main text). Right—field dependence of the magnetization per formula unit.

The value of the product function with the coupling switched off (as assumed at room temperature) for four Dy(III) centers is $\chi T/C_0 = 4 \times 37.78 = 151.1$ (χT = 52.1 cm^3 K mol^{-1} in the cgs and emu units). The observed r.t. value is $\chi T/C_0$ = 118.5 due to the effect that not $J_{max} = 4 \times (15/2) = 60/2$ is the ground molecular state. On cooling, the product function decreases and falls down to the value of 51.9 at T = 2.0 K.

The ground electronic state (multiplet) of a Dy(III) center is $^6H_{15/2}$ with $g_J = 4/3$. Four Dy(III) centers produce $N = 16^4$ = 65,536 magnetic states and M = 2736 zero field states with equal energy. When only the isotropic exchange is considered, the total molecular angular momentum (J) is a good quantum number, and the large-dimensional interaction matrix can be factored to low-dimensional blocks. The molecular values vary between $J_{min} = 0$ and $J_{max} = 4 \cdot (15/2) = 60/2$. Using the technique of irreducible tensor operators [37] the dimensions of these blocks are 16, 45, 71, 94, 114, 131, 145, 156, 164, 169, 171, 170, 166, 159, 149, 136, 120, 105, 91, 78, 66, 55, 45, 36, 28, 21, 15, 10, 6, 3, and 1; these are irrespective of the exchange coupling scheme. The largest dimension M_J = 171 occurs for $J = 20/2$. After the diagonalization of each block, all eigenvalues are collected and inserted to the partition function. A Zeeman term is added to each zero-field energy level for three working fields (this stays diagonal in the basis set of J-manifold assuming a uniform g-factor for each of the Dy centers). Finally, the magnetization and the magnetic susceptibility are calculated by means of statistical thermodynamics as the first and the second field-derivatives of the partition function, respectively.

A reasonable exchange coupling model will require three coupling constants as shown in Table 1. However, in order to avoid an overparameterization and the mu-

tual dependence of the coupling constants, in the simplest model, all of them were set equal. Such a simple exchange coupling model gave the following set of magnetic parameters: J_{ex}/hc = –0.036 (14) cm^{-1}, g = 1.19 (1) and the temperature-independent magnetism χ_{TIM} = 4.9 × 10^{-6} m^3 mol^{-1}; the discrepancy factor of the fit R = 0.077). A release of the constraint for the J-constants gave J_1/hc = –0.0078 cm^{-1}, J_2/hc = –0.094 cm^{-1}, J_3/hc = –0.036 cm^{-1}, g = 1.187 (2) and χ_{TIM} = 4.8 × 10^{-6} m^3 mol^{-1} (R = 0.011). The calculated susceptibility is drawn in Figure 3 as a solid line.

Table 1. Topological matrix for the exchange coupling with the bond angles Dy-O-Dy* in deg [a].

Dy/Dy*	Dy1	Dy2	Dy1*	Dy2*
Dy1	-	*J*1, 107, 112	*J*2, 109	*J*3, 100, 99, 80(Cl)
Dy2		-	*J*3, 100, 99, 80(Cl)	0
Dy1*			-	*J*1, 107, 112
Dy2*				-

[a] According to the core depicted in Figure 1d.

The zero-field energy levels (M = 2736) are displayed in Figure 4 showing that the ground molecular state is J = 0. This explains an observed value of the product function. A further improvement of the model would be based on the zero-field splitting and other crystal-field effects. In such a case, however, there would be the off-diagonal matrix elements mixing the blocks of the different angular momentum so that the blocking of the interaction matrix is not possible anymore.

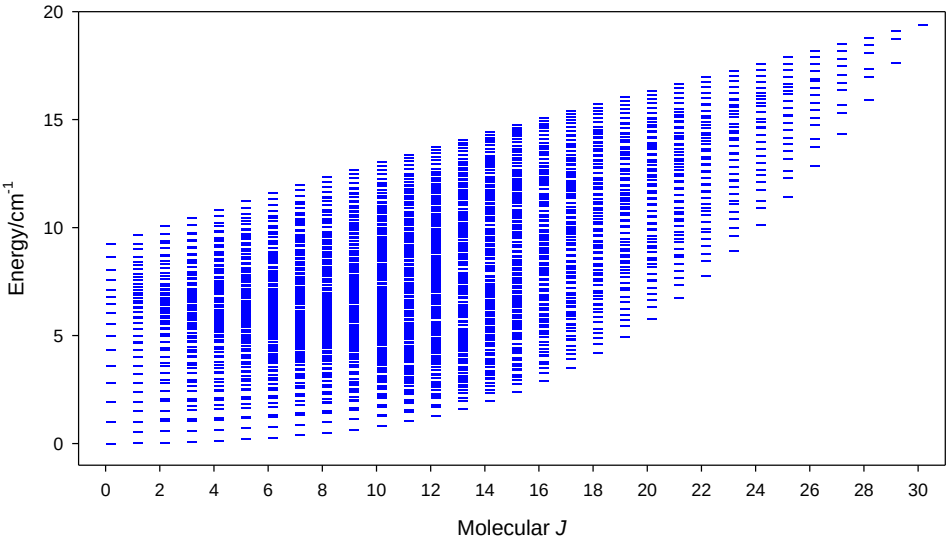

Figure 4. Calculated energy spectrum of **1**.

2.3. AC Susceptibility

In order to test a possible slow magnetic relaxation in **1**, AC susceptibility measurements were performed using the small amplitude of the oscillating field B_{AC} = 0.3 mT, at T = 2 K for a variable set of frequencies f = 1 − 1488 Hz, and applied external field B_{DC} = 0 to 0.5 T; the results are presented in Figure 5. The out-of-phase susceptibility is non-zero even in the absence of the external field. This means that 1 behaves as a true single molecule magnet. With increasing external field, the profile of χ'' alters.

Both AC susceptibility components were fitted simultaneously by employing the two-set Debye model. This model contains seven free parameters: a pair of isothermal susceptibilities χ_{T1} and χ_{T2}, two distribution parameters α_1 and α_2, two relaxation times τ_1 (low-frequency, LF) and τ_2 (high-frequency, HF) and the common adiabatic susceptibility χ_S. At T = 2.0 K and B_{DC} = 0, the relaxation times are τ_{LF} = 29 ms and τ_{HF} = 75 µs, and the mole fraction x_{LF} = 0.24 (x_{HF} = 1 − x_{LF}). With B_{DC} = 0.5 T, these parameters alter to

τ_{LF} = 9 ms and τ_{HF} = 66 μs, and x_{LF} = 0.52. To this end, **1** is the single-molecule magnet even in the absence of the external magnetic field.

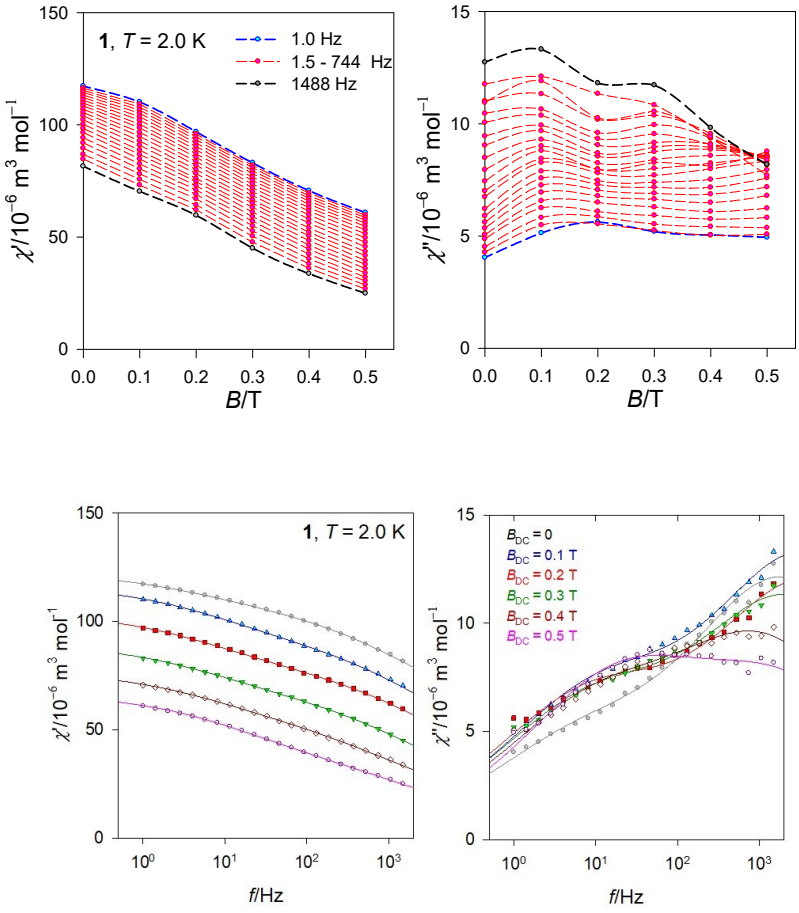

Figure 5. Field dependence (**top**) and frequency dependence (**bottom**) of the AC susceptibility components for **1** at T = 2.0 K. Dashed—guide for eyes; solid lines—fitted.

The temperature dependence of the AC susceptibility for various frequencies of the oscillating field at B_{DC} = 0 is shown in Figure 6. It is seen that the out-of-phase susceptibility survives until T > 10 K.

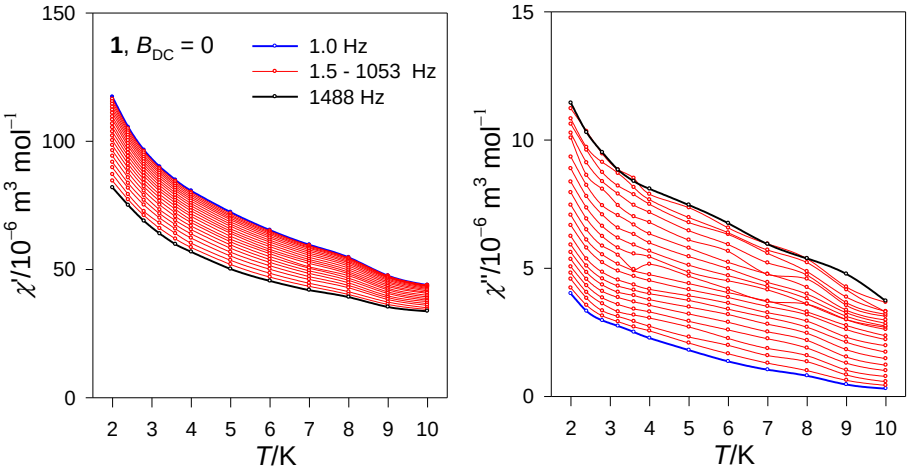

Figure 6. Temperature dependence of the AC susceptibility for **1**.

The same dataset has been rearranged as a frequency dependence of the AC susceptibility for a set of temperatures as shown in Figure 7. This function can be fitted to the two-set Debye model, since two relaxation channels are evident: the low-frequency (LF) and the high-frequency (HF) one.

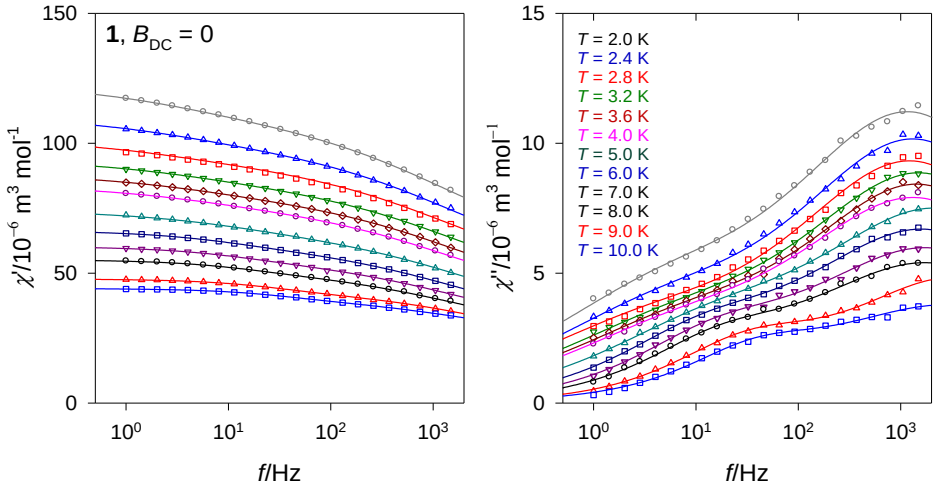

Figure 7. The frequency dependence of the AC susceptibility for **1**. Solid lines—fitted.

Temperature evolution of the (fitted) relaxation time, individually for the LF and HF relaxation channels, is presented in Figure 8. It can be seen that the HF relaxation time below 8 K is almost temperature independent, which indicates a quantum tunnelling relaxation process.

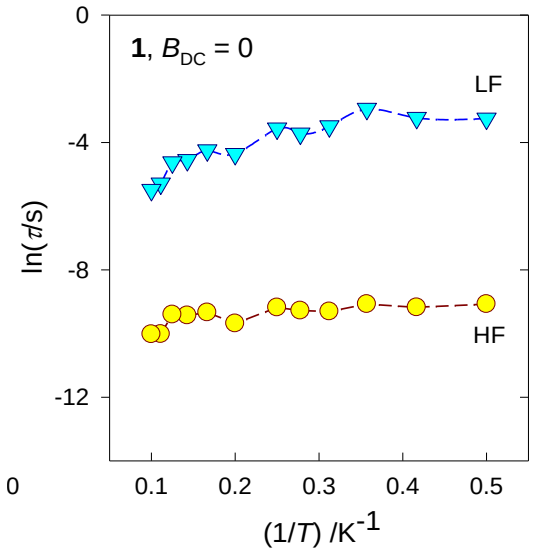

Figure 8. Arrhenius like plot of lnτ vs. T^{-1} for **1**.

3. Materials and Methods

3.1. General Procedures

All the starting materials, *o*-vanillin, 2-(aminomethyl)pyridine, triethylamine, dysprosium chloride hexahydrate and solvents were of analytical reagent grade and were used without any further purification.

Elemental analysis for C, H, and N was carried out on a Flash 2000 CHNSO apparatus (Thermo Scientific). FTIR spectra were measured by the ATR method in the region of 400–4000 cm^{-1} (Shimadzu IR Affinity^{-1}, Quest ATR holder).

Magnetic susceptibility data were collected at temperatures between 2 and 300 K using a Quantum Design MPMS-XL SQUID magnetometer equipped with a 1 T magnet at an external field of 0.1 T. The samples were grounded and fixed in a gelatine capsule using small amounts of eicosane to avoid any movement of the sample. The data obtained were corrected for diamagnetic contributions of the sample, the eicosane, the gelatine capsule and the sample holder.

*3.2. Synthesis of Tetranuclear Dysprosium Complex (**1**)*

The tetranuclear complex ($C_{56}H_{54}Cl_6Dy_4N_8O_{10}$) (1) (Scheme 1) was synthesized by slowly adding a methanol solution of $DyCl_3 \cdot 6H_2O$ (1.0 mmol, 0.376 g) dissolved in 15 mL into a stirring solution of *o*-vanillin (1 mmol, 0.152 g) and 2-(aminomethyl)pyridine (1 mmol, 0.108 mL) in the presence of triethylamine (1 mmol, 0.101 mL) in methanol (50 mL). The mixture was refluxed for 4 h in an oil bath. The yellow solution obtained on reflux was cooled to room temperature and filtered. Vapor diffusion of diethyl ether to the filtered yellow solution yielded X-ray quality yellow block crystals. The complex was collected by filtration and washed with cold MeOH and dried in air and vacuum. Yield, 200 mg, 52.25%. Anal. Calc. for **1,** 38.97 (C), 7.15 (N), 4.95 (H); Found: 38.84 (C), 7.02 (N), 4.42 (H). IR (KBr disc)/cm^{-1}: 2981.25 (w), 2943.44 (w), 2609.96 (m), 2496.53 (m), 2358.15 (m), 2333.20 (w), 1634.48 (s), 1558.86 (m), 1508.95 (m), 1464.34 (s), 1301 (m), 1212.53 (s), 1168.67 (m), 1036.34 (s), 961.48 (w), 854.10 (w), 740.67 (w), 627.24 (m), 552.38 (m), 413.24 (s).

3.3. X-ray Crystallography

Single crystal X-ray diffraction measurements were performed on a STOE StadiVadi 25 diffractometer using a GeniX 3D HF micro focus with MoKα-radiation (λ = 0.71073 Å) and a CCD image plate detector. The crystals were mounted using crystallographic oil and placed in a cold nitrogen stream. All the data were corrected for absorption using CrysAlisPro [38]. The structures were solved by direct methods and refined against F^2 using the SHELXL-97 package [39] in Olex2.25. All non-hydrogen atoms were refined anisotropically, and hydrogens were placed based on a riding model approach. Full crystallographic details can be found in CIF format: see the Cambridge Crystallographic Data Centre database 2161049 for complex **1.** Crystal parameters and refinement results for the complex are collated in Table S2, and the selected bond lengths and bond angles of complex **1** are presented in Table S1.

4. Conclusions

In summing up, a tetranuclear dysprosium Schiff base complex was synthesized and characterized by single crystal XRD, elemental analysis and molecular spectroscopy. DC susceptibility measurements of the aggregate reveal an antiferromagnetic behavior of the complex. AC susceptibility proves that the complex is exhibiting single molecule magnetic behavior, showing slow magnetic relaxation at zero field. As the coordination environments clearly change the anisotropic nature of the four dysprosium ions, the present case opens ample opportunities to play around the anisotropy by changing the coordination environment, introducing new ligand functionalities as bridging or by coordination capacities. In general, we are expecting that the present work with modified ligand architecture will be promising to design and synthesize dysprosium-based single molecule magnets with superior characteristics.

Supplementary Materials: The following supporting information can be downloaded at: https://www.mdpi.com/article/10.3390/inorganics10050066/s1, Figure S1: View on intermolecular contacts formed in complex 1 through the building of extended networks in the three crystallographic directions (along a, along b and along c); Table S1: Selected bond lengths (Å) and bond angles (°) in 1; Table S2: Crystal data and structure refinement for **1**.

Author Contributions: The major work for this article, designing, execution and writing of the original draft, was completed by the first author: M.G., which is part of his Ph.D. program. The second author: S.S. participated in characterizations (solving the structure and SQUID measurement). The remaining authors: C.R., A.S., M.R., M.T. and R.B. were responsible for supervision, editing, and reviewing of this article. In addition, the authors: C.R., M.R. and R.B. have completed the DC and AC data analysis of the compound. All authors have read and agreed to the published version of the manuscript.

Funding: This research project was supported by the National Scholarship Programme of the Slovak Republic 2021 and Addis Ababa Science and Technology University, Ethiopia for (M.G). Financial support of Slovak grants agencies (APVV 18-0016, APVV 19-0087, VEGA 1/0191/22 and VEGA 1/0086/21) are thankfully acknowledged.

Institutional Review Board Statement: Not applicable.

Informed Consent Statement: Not applicable.

Data Availability Statement: Not applicable.

Acknowledgments: We are thankful to National Scholarship Programme of the Slovak Republic 2021 for a research stay and Addis Ababa Science and Technology University, Ethiopia for a Ph.D. studentship for M.G. We acknowledge our thankfulness to R. Mičová UCM, Trnava, Slovakia, for the spectroscopic and microanalysis. We are also thankful to S. Klyatskaya from KIT, Germany for her support during this work.

Conflicts of Interest: The authors declare no conflict of interest.

References

1. Gatteschi, D.; Sessoli, R.; Villain, J. *Molecular Nanomagnets*; Oxford University Press: Oxford, UK, 2006; ISBN 9780191718298.
2. Ritter, S.K. Single-molecule magnets evolve. *Chem. Eng. News* **2004**, *82*, 29–32. [CrossRef]
3. Layfield, R.A.; Murugesu, M. *Lanthanides and Actinides in Molecular Magnetism*; John Wiley & Sons: Hoboken, NJ, USA, 2015; ISBN 9781119950837.
4. Sessoli, R.; Gatteschi, D.; Caneschi, A.; Novak, M.A. Magnetic bistability in a metal-ion cluster. *Nature* **1993**, *365*, 141–143. [CrossRef]
5. Ishikawa, N.; Sugita, M.; Ishikawa, T.; Koshihara, S.; Kaizu, Y. Lanthanide Double-Decker Complexes Functioning as Magnets at the Single-Molecular Level. *J. Am. Chem. Soc.* **2003**, *125*, 8694–8695. [CrossRef] [PubMed]
6. Zhang, P.; Zhang, L.; Tang, J. Lanthanide single molecule magnets: Progress and perspective. *Dalt. Trans.* **2015**, *44*, 3923–3929. [CrossRef] [PubMed]
7. Woodruff, D.N.; Winpenny, R.E.P.; Layfield, R.A. Lanthanide Single-Molecule Magnets. *Chem. Rev.* **2013**, *113*, 5110–5148. [CrossRef]
8. Boča, R.; Stolárová, M.; Falvello, L.R.; Tomás, M.; Titiš, J.; Černák, J. Slow magnetic relaxations in a ladder-type Dy(III) complex and its dinuclear analogue. *Dalt. Trans.* **2017**, *46*, 5344–5351. [CrossRef] [PubMed]
9. Dolai, M.; Ali, M.; Rajnák, C.; Titiš, J.; Boča, R. Slow magnetic relaxation in Cu(ii)-Eu(iii) and Cu(ii)-La(iii) complexes. *New J. Chem.* **2019**, *43*, 12698–12701. [CrossRef]
10. Hazra, S.; Titiš, J.; Valigura, D.; Boča, R.; Mohanta, S. Bis-phenoxido and bis-acetato bridged heteronuclear {CoIIIDyIII} single molecule magnets with two slow relaxation branches. *Dalt. Trans.* **2016**, *45*, 7510–7520. [CrossRef]
11. Luzon, J.; Sessoli, R. Lanthanides in molecular magnetism: So fascinating, so challenging. *Dalt. Trans.* **2012**, *41*, 13556–13567. [CrossRef]
12. Sorace, L.; Benelli, C.; Gatteschi, D. Lanthanides in molecular magnetism: Old tools in a new field. *Chem. Soc. Rev.* **2011**, *40*, 3092–3104. [CrossRef]
13. Liddle, S.T.; Slageren, J. van Improving f-element single molecule magnets. *Chem. Soc. Rev.* **2015**, *44*, 6655–6669. [CrossRef] [PubMed]
14. Habib, F.; Murugesu, M. Lessons learned from dinuclear lanthanide nano-magnets. *Chem. Soc. Rev.* **2013**, *42*, 3278–3288. [CrossRef]
15. Pinkowicz, D.; Southerland, H.I.; Avendan, C.; Prosvirin, A.; Sanders, C.; Wernsdorfer, W.; Pedersen, K.S.; Dreiser, J.; Cle, R.; Nehrkorn, J.; et al. Cyanide Single-Molecule Magnets Exhibiting Solvent Dependent Reversible "On" and "Off " Exchange Bias Behavior. *J. Am. Chem. Soc.* **2015**, *45*, 14406–14422. [CrossRef] [PubMed]
16. Dreiser, J. Molecular lanthanide single-ion magnets: From bulk to submonolayers. *J. Phys. Condens. Matter* **2015**, *27*, 183203. [CrossRef] [PubMed]
17. Lin, S.Y.; Tang, J. Versatile tetranuclear dysprosium single-molecule magnets. *Polyhedron* **2014**, *83*, 185–196. [CrossRef]

18. Vráblová, A.; Tomás, M.; Falvello, L.R.; Dlháň, Ľ.; Titiš, J.; Černák, J.; Boča, R. Slow magnetic relaxation in Ni-Ln (Ln = Ce, Gd, Dy) dinuclear complexes. *Dalt. Trans.* **2019**, *48*, 13943–13952. [CrossRef]
19. Moreno-Pineda, E.; Godfrin, C.; Balestro, F.; Wernsdorfer, W.; Ruben, M. Molecular spin qudits for quantum algorithms. *Chem. Soc. Rev.* **2018**, *47*, 501–513. [CrossRef]
20. Peng, J.B.; Kong, X.J.; Zhang, Q.C.; Orendáč, M.; Prokleška, J.; Ren, Y.P.; Long, L.S.; Zheng, Z.; Zheng, L.S. Beauty, symmetry, and magnetocaloric effect-four-shell keplerates with 104 lanthanide atoms. *J. Am. Chem. Soc.* **2014**, *136*, 17938–17941. [CrossRef]
21. Vincent, R.; Klyatskaya, S.; Ruben, M.; Wernsdorfer, W.; Balestro, F. Electronic read-out of a single nuclear spin using a molecular spin transistor. *Nature* **2012**, *488*, 357–360. [CrossRef]
22. Gebrezgiabher, M.; Bayeh, Y.; Gebretsadik, T.; Gebreslassie, G.; Elemo, F.; Thomas, M.; Linert, W. Lanthanide-based single-molecule magnets derived from schiff base ligands of salicylaldehyde derivatives. *Inorganics* **2020**, *8*, 66. [CrossRef]
23. Senthil Kumar, K.; Bayeh, Y.; Gebretsadik, T.; Elemo, F.; Gebrezgiabher, M.; Thomas, M.; Ruben, M. Spin-crossover in iron(ii)-Schiff base complexes. *Dalt. Trans.* **2019**, *48*, 15321–15337. [CrossRef] [PubMed]
24. Khan, A.; Akhtar, M.N.; Lan, Y.; Anson, C.E.; Powell, A.K. Linear shaped hetero-metallic [Zn_2Ln_4] clusters with Schiff base ligand: Synthesis, characterization and magnetic properties. *Inorg. Chim. Acta* **2021**, *524*, 5–10. [CrossRef]
25. Khan, A.; Fuhr, O.; Akhtar, M.N.; Lan, Y.; Thomas, M.; Powell, A.K. Synthesis, characterization and magnetic studies of dinuclear lanthanide complexes constructed with a Schiff base ligand. *J. Coord. Chem.* **2020**, *73*, 1045–1054. [CrossRef]
26. Wang, H.L.; Peng, J.M.; Zhu, Z.H.; Mo, K.Q.; Ma, X.F.; Li, B.; Zou, H.H.; Liang, F.P. Step-by-Step and Competitive Assembly of Two Dy(III) Single-Molecule Magnets with Their Performance Tuned by Schiff Base Ligands. *Cryst. Growth Des.* **2019**, *19*, 5369–5375. [CrossRef]
27. Maxim, C.; Pasatoiu, T.D.; Kravtsov, V.C.; Shova, S.; Muryn, C.A.; Winpenny, R.E.P.; Tuna, F.; Andruh, M. Copper(II) and zinc(II) complexes with Schiff-base ligands derived from salicylaldehyde and 3-methoxysalicylaldehyde: Synthesis, crystal structures, magnetic and luminescence properties. *Inorg. Chim. Acta* **2008**, *361*, 3903–3911. [CrossRef]
28. Patil, S.A.; Weng, C.M.; Huang, P.C.; Hong, F.E. Convenient and efficient Suzuki-Miyaura cross-coupling reactions catalyzed by palladium complexes containing N,N,O-tridentate ligands. *Tetrahedron* **2009**, *65*, 2889–2897. [CrossRef]
29. Llunell, S.A.M.; Casanova, D.; Cirera, J.; Alemany, P.; Alvarez, S. *SHAPE-Program for the Stereochemical Analysis of Molecular Fragments by Means of Continuous Shape Measures and Associated Tools Version 2.1*; Universitat de Barcelona: Barcelona, Spain, 2013.
30. Zheng, Y.Z.; Lan, Y.; Anson, C.E.; Powell, A.K. Anion-perturbed magnetic slow relaxation in planar {Dy4} clusters. *Inorg. Chem.* **2008**, *47*, 10813–10815. [CrossRef]
31. Langley, S.K.; Chilton, N.F.; Gass, I.A.; Moubaraki, B.; Murray, K.S. Planar tetranuclear lanthanide clusters with the Dy4 analogue displaying slow magnetic relaxation. *Dalt. Trans.* **2011**, *40*, 12656–12659. [CrossRef]
32. Abbas, G.; Lan, Y.; Kostakis, G.E.; Wernsdorfer, W.; Anson, C.E.; Powell, A.K. Series of isostructural planar lanthanide complexes [LnIII4(μ3-OH)2(mdeaH)2(piv) 8] with single molecule magnet behavior for the Dy4 analogue. *Inorg. Chem.* **2010**, *49*, 8067–8072. [CrossRef]
33. Jami, A.K.; Ali, J.; Mondal, S.; Homs-Esquius, J.; Sañudo, E.C.; Baskar, V. Dy2 and Dy4 hydroxo clusters assembled using o-vanillin based Schiff bases as ligands and β-diketone co-ligands: Dy4 cluster exhibits slow magnetic relaxation. *Polyhedron* **2018**, *151*, 90–99. [CrossRef]
34. Lin, P.H.; Burchell, T.J.; Ungur, L.; Chibotaru, L.F.; Wernsdorfer, W.; Murugesu, M. A polinuclear lanthanide single-molecule magnet with a record anisotropic barrier. *Angew. Chemie-Int. Ed.* **2009**, *48*, 9489–9492. [CrossRef] [PubMed]
35. Kuang, W.W.; Zhu, L.L.; Xu, Y.; Yang, P.P. A tetranuclear holmium compound exhibiting single molecule magnet behavior. *Inorg. Chem. Commun.* **2015**, *61*, 169–172. [CrossRef]
36. Yan, P.F.; Lin, P.H.; Habib, F.; Aharen, T.; Murugesu, M.; Deng, Z.P.; Li, G.M.; Sun, W. Bin Planar tetranuclear dy(III) single-molecule magnet and its Sm(III), Gd(III), and Tb(III) analogues encapsulated by salen-type and β-diketonate ligands. *Inorg. Chem.* **2011**, *50*, 7059–7065. [CrossRef] [PubMed]
37. Boča, R. *A Handbook of Magnetochemical Formulae*; Elsevier: Amsterdam, The Netherlands, 2012; ISBN 978-0-12-416014-9.
38. *Agilent, CrysAlisPro Data Collection and Processing Software for Agilent X-ray Diffractometers*; Technol. UK Ltd.: Oxford, UK, 2014; Volume 44, pp. 1–53.
39. Sheldrick, G.M. A short history of SHELX. *Acta Crystallogr. Sect. A Found. Crystallogr.* **2008**, *64*, 112–122. [CrossRef]